

# **An Investigation of the Effect of Pre-Straining on the Creep Behaviour of a P91 Steel at 600°C using Impression Creep Testing**

Brett SJ, Dyson C, Maskill S, Bridges A, Sun W

## **Abstract:**

This paper investigates the effect of high temperature tensile strain on subsequent creep strength in a grade 91 steel using impression creep testing. The grade 91 material investigated has been tested in two different microstructural conditions, in the normal martensitic condition and in an aberrant mis-heat treated condition in which the microstructure is 100% ferrite. The latter condition is of interest because of its widespread occurrence on operating power plant. The two microstructural conditions were confirmed by hardness mapping and Electron Back Scattered Diffraction (EBSD). Previous investigations have used pre-strained uniaxial creep specimens to investigate this effect, but the present work has utilised the specialised small-scale impression creep testing technique to test material obtained at a number of positions along the axes of failed hot tensile specimens. This allowed impression creep samples to be extracted at various pre-strains for investigation and for a wide range of hot tensile pre-strain to be investigated. The two microstructural conditions have shown a divergence in behaviour, with the normal martensitic material showing little change in creep strength with increasing pre-strain and the aberrant material increasing markedly in creep strength with increasing pre-strain.

**Keywords:** Pre-Straining, Impression Creep, P91 Steel, Normal and Aberrant Microstructure

## **1. Background**

### **1.1 Strain Induced in Components During Manufacture**

Strain introduced into components during the manufacturing process may survive into subsequent service, affecting material properties such as creep, and previous work in this area has considered the possible enhancement of creep properties by pre-straining [1]. The process of hot bending steam pipe for example involves substantial deformation, producing wall thinning at the bend extrados and wall thickening at the bend intrados, resulting potentially in a significant variation in creep properties. There have been a few studies in recent years on the effect of pre-

straining on stainless steel 316H [2]–[4], where it has been shown to increase creep resistance. Nickel based alloys have also been tested where the opposite effect has been present [5]. It has been shown that, depending on the material composition, the effect of pre-straining may have either enhanced or deleterious effects on the creep strain rate, creep ductility and rupture life of the material [6].

The present work has investigated a grade 91 material in two different heat-treated conditions. One form is the as-manufactured normal condition, with 100% martensite, while the other is an artificially mis heat-treated condition with 100% ferrite. Although it is acknowledged that the detailed precipitate and dislocation microstructure will be different in the two forms, this has not been specifically investigated. It is considered that the presence or absence of martensite will be the dominant factor controlling creep strength.

Previous work on pre-straining focused on testing pre-strained uniaxial specimens in the creep regime [15]. In this case only the engineering strain was taken into account and so it is not known how the true strain affected the creep results. In order to obtain creep data at specific true strain levels, impression creep testing of sections of plastically deformed uniaxial test specimens was utilised in the present work. This approach makes it easier to investigate more localised creep behaviour in systems where the pre-straining is not uniform, similar to the way in which the test method has been used to characterise weldments [7]. The novelty in testing is the opportunity to remove material for impression specimens from the elongated gauge section of a failed hot tensile specimen at points of specific strain. In principle material can be sampled at the highest tensile strain immediately adjacent to the fracture point although, because of the severe deformation in this region, the strain value in this case will be approximate.

## 1.2 Impression Creep Testing

The impression creep test [8]–[10] is a small-scale technique similar to, but distinctly different from the Small Punch test [11]–[13]. The Small Punch test uses a circular disc specimen that is 8mm in diameter and 0.5mm thick, which is indented with a spherical indenter. This is further described in a CEN workshop agreement [14]. The impression creep test typically uses 10x10mm rectangular specimens that are 2.5 mm thick, which are indented with a flat rectangular indenter having a contact area 10x1mm. An example of the specimen geometry and loading set-up can be seen in Figure 1. The impression creep test is the simpler of the two tests in that the specimen is deformed in uniaxial compression at constant stress and contact area. A benefit of this simplicity is that the conversion of the test data into equivalent uniaxial creep data is relatively

straightforward. In the present work, the effect of pre-straining on subsequent creep strength was investigated using the impression creep test on the normal and mis-heat treated P91.

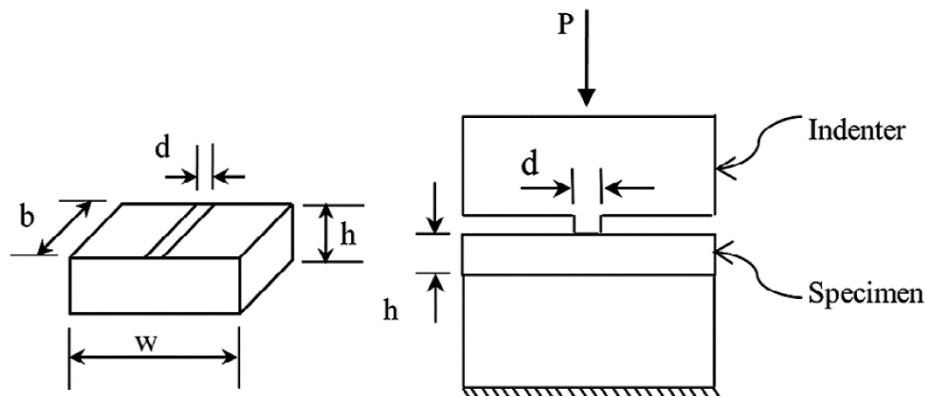


**Figure 1: Left impression specimen, right impression loading arrangement.**

### 1.3 P91 Steel – Normal and Aberrant Microstructural Conditions

P91 steel is a high chromium power plant steel with enhanced creep strengthening derived from fine niobium vanadium carbo-nitride (MX type) precipitation. It is characterised by its martensitic microstructure, produced by heat treatment which typically involves austenitizing in the temperature range 1040-1080°C, air-cooling, and then tempering in the range 730-800°C [16]. It is used primarily in forgings, tubing, pipes and headers. If mis-heat treated, P91 may fail to achieve a fully martensitic microstructure. Its microstructure may become mixed martensitic and ferritic or, in the worst cases, 100% ferrite. In this latter form it is often referred to as “aberrant” P91. If found in-service aberrant P91 presents a risk to power plant operators because the absence of martensite results in a creep strength substantially lower than that of correctly heat-treated material. It is often detected in service because of its low hardness, typically 160HV or less in comparison to 200-250HV for normal P91.

## **2. Material and Experimental Set-Up**

### **2.1 Material and Heat Treatment**

Although it may not always be possible to establish how the aberrant microstructure has formed in individual cases, an absence of martensite implies that, at some stage, temperature has risen into the austenite range. The most likely way this can occur is by overshooting the tempering temperature either during the tempering stage of parent material production or during the post weld heat treatment of a weld. If the temperature rises sufficiently into the austenite range before falling back to the correct tempering temperature, the martensite can disappear. The tempering or post weld heat treatment will then be carried out on a ferrite microstructure, which will be retained on final cooling to ambient.

A series of trials by Heywood [17] has shown that one particular heat treatment sequence can successfully reproduce the aberrant microstructure observed in service, and this was used in the present work.

A sample of the normal martensitic P91 was first austenitized in a furnace at 910°C for 30mins. The temperature of the furnace was then reduced to 760°C and the sample held at this temperature for 3.5hrs. This ensured that the 100% ferrite microstructure was fully formed throughout the thickness of the sample. After the 3.5hr holding period the sample was left in the furnace to cool down slowly to room temperature. Finally, hardness testing of the sample was used to confirm that aberrant material had been produced.

### **2.2 Large Uniaxial Specimen and Hot Tensile Testing**

Uniaxial hot tensile tests were carried out on the normal and aberrant versions of the P91 material at 600°C and a strain rate of 0.025% per second. The tests were carried out to failure and true strain values calculated using FE analysis. A specimen with a gauge length/diameter ratio of 5/1, identical to that of the standard uniaxial creep specimen was tested. The largest available hot tensile specimen (M20) was utilized, corresponding to a gauge diameter of 16mm. Details of the uniaxial specimen used can be seen in Figure 2.

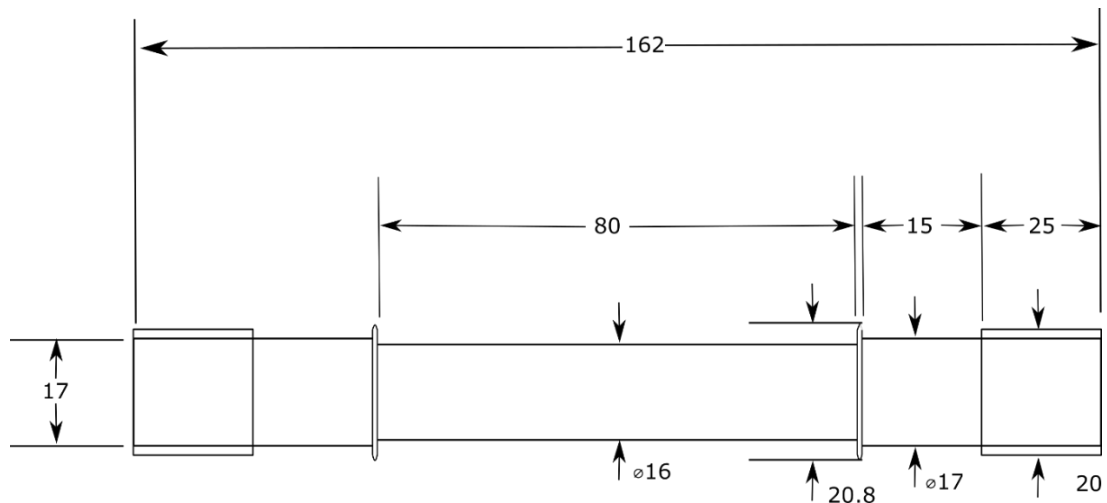


**Figure 2: Oversize uniaxial specimen (dimensions in mm)**

### 2.3 Removal of Impression Specimen and Creep Testing

Once the uniaxial specimen had fractured, impression specimens were removed from four locations and the grip, at distances shown in Table 1. The error shown in the calculated true strain reflects the residual stress caused by the cutting and the width of the cuts themselves. The impression specimen removed from the grip of the hot tensile specimen can be regarded as an un-strained control specimen. The strains at the impression specimen locations were estimated preliminarily using diametrical measurements using equation (1) and calculated by the FE Model:

$$R_A = 1 - e^{\varepsilon_t} \quad (1)$$

where  $R_A$  is the reduction in area ratio and  $\varepsilon_t$  is the true strain. During machining of the impression specimens it was ensured that “witness marks” were left on the specimen in order that the surface closest to the fracture site could be used as the loading surface in the subsequent impression creep test. The specimens were tested at a converted impression test stress of 98 MPa, falling in the power law creep regime, with a duration of ~250hrs for each test.

**Table 1: Strain levels and locations of removed material for both specimens**

Aberrant			Martensitic		
True strain (abs)	Distance from failure site (mm)	$R_A$	True strain (abs)	Distance from failure site (mm)	$R_A$
0	50	0	0	50	0
0.12±0.008	46	0.09	0.14±0.009	13	0.23
0.41±0.025	11	0.26	0.31±0.022	9	0.31
0.60±0.069	7	0.38	0.60±0.064	6	0.38

### 3. Experimental Results at 600°C

#### 3.1 Uniaxial Tensile Test

The aberrant material had a higher ductility than the martensitic material at the test temperature, the engineering strain increasing by a factor of 1.5. The more pronounced necking in the aberrant uniaxial specimen however made it more difficult to remove impression specimens in material with the largest strains.

The relationship between engineering stress and strain can be easily derived:

$$\varepsilon_t = \int_{l_0}^l \frac{dl}{l} = \ln\left(\frac{l}{l_0}\right) = \ln\left(\frac{A_0}{A}\right) = \ln(1 + \varepsilon_{eng}) \quad (2)$$

and the true stress  $\sigma_t$ :

$$\sigma_t = \sigma_{eng}(1 + \varepsilon_{eng}) \quad (3)$$

necking is not considered, so these relationships hold up until the ultimate tensile stress of the material from which point the material is assumed to obey the simple isotropic hardening law:

$$\sigma_t = K\varepsilon_t^m \quad (4)$$

The constants  $K$  and  $m$  can be obtained by taking the logs of the plastic portion of the true stress-strain curve and taking the intercept and gradient respectively, in this case they were found to be  $K=329.7$  MPa and  $m = 0.1272$ , for aberrant and  $K=518.7$  MPa and  $m=0.1002$  for martensitic. It is clear from Figure 3 that the martensitic material is considerably stronger in tension and has a much lower ductility compared to the aberrant (ferritic) material

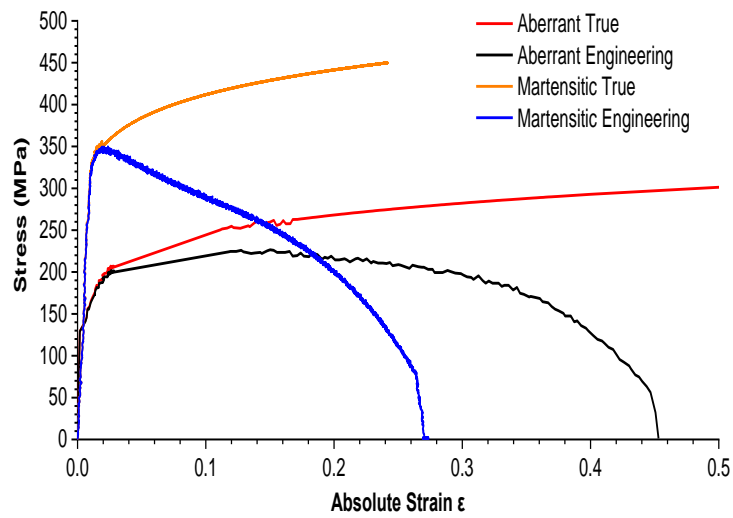


**Figure 3: Engineering and True stress and strain curves for both microstructures at 600°C**

### 3.2 EBSD and Hardness Mapping of Tested Tensile Specimen

An Electron Back Scattered Diffraction (EBSD) image of the martensitic specimen taken from near the grip is shown below in Figure 4. The distinctive martensite lath structure can be clearly seen.

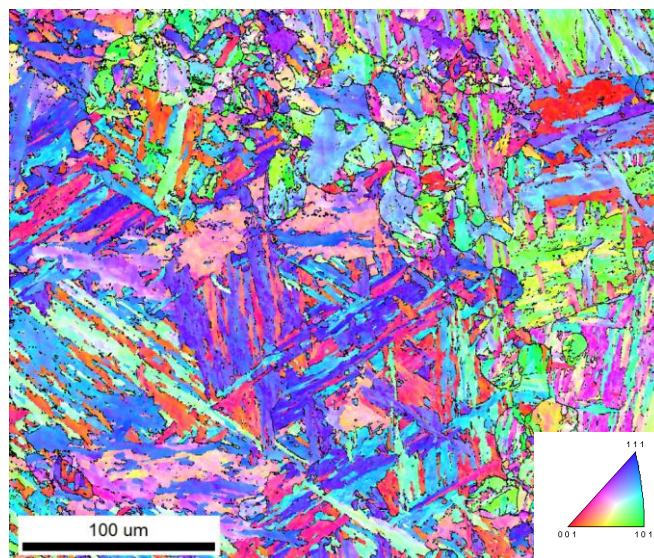


**Figure 4: EBSD inverse pole figure of martensitic specimen near grip**

EBSD and hardness mapping of the two failed hot tensile specimens are shown in Figure 5. The EBSD shows clearly that, in contrast to the normal material, the aberrant condition has a martensite lath-free 100% ferrite structure. Hardness mapping was used as an initial indicator of

strain variation within the gauge lengths of the failed specimens in order to select the axial positions from which to remove the impression specimens. While, as might be expected, the hardness of the aberrant hot tensile specimen was lower than that of the normal specimen, for both hot tensile specimens little variation in hardness was found between the grip and the gauge section furthest from the fracture site. In both cases hardness increased in the direction of the fracture site, as necking increased (Figure 5). The EBSD images shown were taken at approximately the 25-30mm distance shown on the hardness plots in Figure 5, within the necked regions of the specimens, but away from the fracture sites.

In the case of the aberrant hot tensile specimen the increase in hardness in the gauge length compared to the grip is in contrast with behaviour observed in a microstructurally similar failed uniaxial creep specimen. A creep specimen in ex-service failed CrMoV, also 100% ferrite, showed no variation in hardness between the grip and the fracture location [18].

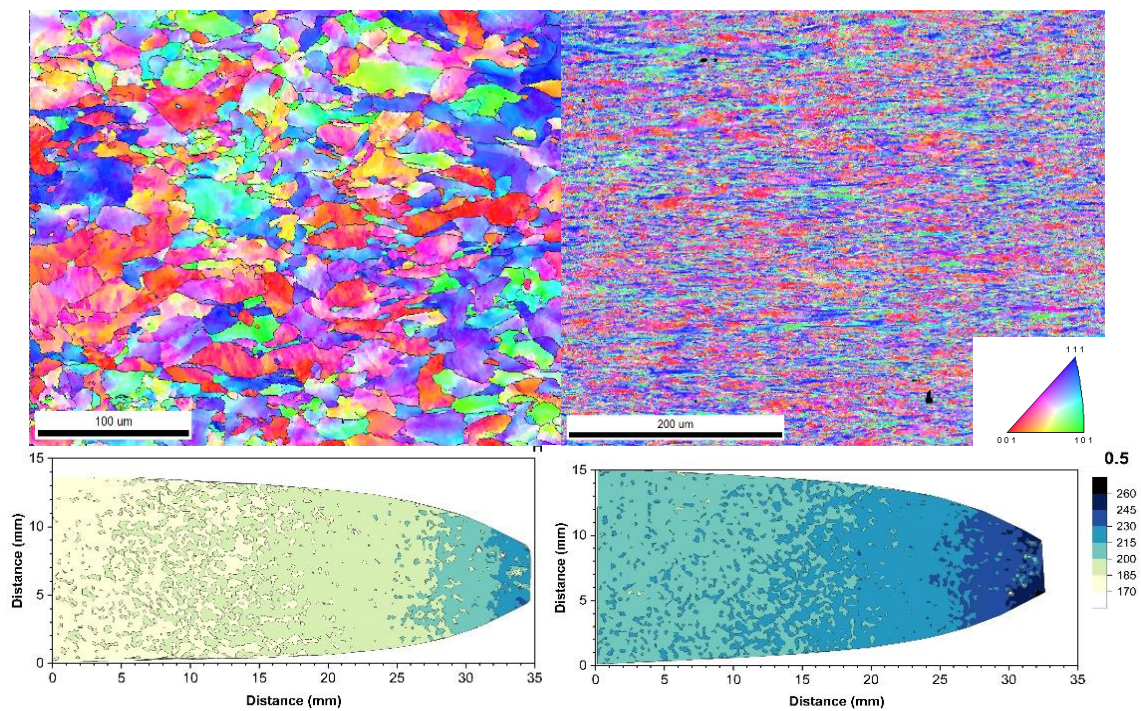


**Figure 5: SEM-EBSD inverse pole figures and legend for aberrant (top left) martensite (top right) and hardness maps for failed specimens aberrant (bottom left) martensite (bottom right)**

### 3.3 Impression Creep Tests Using Un-Strained and Pre-Strain Specimens

The impression creep results for pre-strains as calculated in Section 2.3 are shown in Figure 6. The plots of indentation depth with time are typical of impression creep tests, with the indentation rate gradually approaching a near constant value. Equivalent minimum creep strain rates were calculated within a 100-hour window for each material, which is the slope at 134-234hrs for the aberrant tests and 150-250hrs for the martensitic traces. Strain rate-time data is the 100-hour slope taken at each point as a reference through the window.

The impression creep strain rate in the normal martensitic material remains largely unchanged as the pre-strain increases. For the aberrant material, in contrast, the impression creep strain rate decreases steadily with pre-strain. While the two materials show a large difference in impression creep strain rate at no pre-strain, they become very similar at the highest levels of pre-strain.

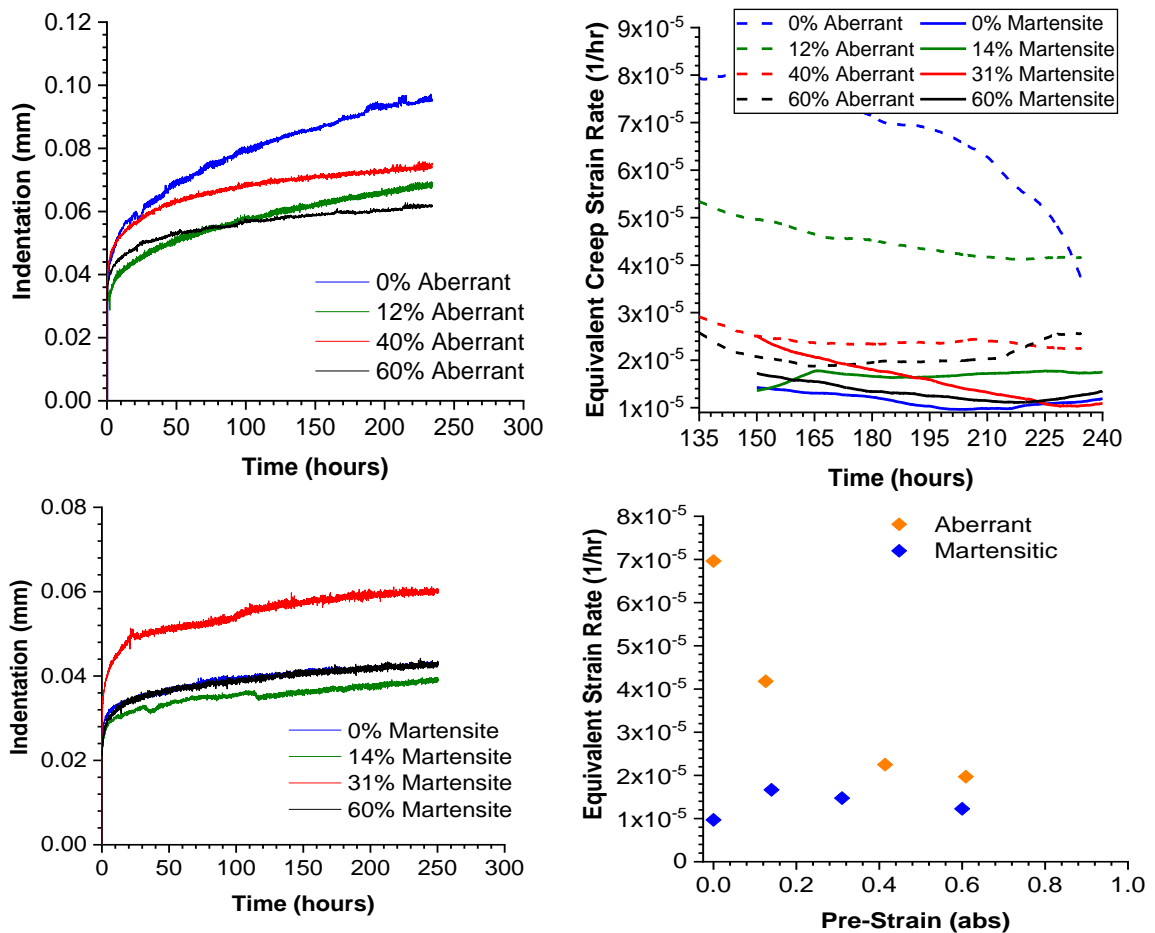


**Figure 6: Impression creep test results at different pre-strains for P91 at 98 MPa 600°C (left) aberrant (top) and martensite (bottom). Creep strain rates (right) plotted against time (top) and pre-strain (bottom)**

#### 4. Finite Element Modelling of Large Uniaxial Tensile Test

The hot tensile test specimen was simulated using the finite element method in order to accurately calculate the strains within the specimen at failure using an elastic-plastic analysis. A basic constitutive relation was used to describe the plastically deformed specimen with the total strain being described as a combination of elastic and plastic strains:

$$\varepsilon = \varepsilon^{el} + \varepsilon^{pl} \quad (5)$$

The material exhibits plastic flow when the yield stress is exceeded following a power law relationship,

$$\dot{\varepsilon} = D(\dot{q}/\sigma^0 - 1)^n \quad (6)$$

where  $\dot{\varepsilon}$  is the equivalent plastic strain rate  $q$  is the equivalent stress,  $\sigma^0$  is the material yield stress and  $D, n$  are temperature dependant material parameters. The plastic strain increment is calculated numerically using the flow rule,

$$\Delta \mathbf{e}^{pl} = \Delta \bar{\varepsilon}^{pl} \frac{3}{2} \mathbf{S} / q \quad (7)$$

where,  $\mathbf{S}$  is the deviatoric stress tensor and  $\Delta \bar{\varepsilon}^{pl}$  is the scalar equivalent plastic strain. The commercial numerical software Abaqus was used simulating a quarter of the specimen with the in-built plasticity model, using a uniform element size in the gauge section. Axisymmetric quad reduced integration elements were used in order to allow for smooth deformation of the 0.5mm elements in the necked region selected after a mesh study. The geometry non-linear feature was also used to account for the large deformations near the failure site and the accompanying necking in the sample. During this mode the Jacobian is constantly updated as the elements undergo severe stretching around the centre of the specimen and the stress state of the specimen transforms from purely uniaxial to a triaxial state of stress. The simulation is run to the equivalent plastic strain and triaxial stress factor at failure. Failure being the engineering strain at which the experimental sample failed. The model gives a good prediction of the deformation characteristics of the material as seen in Figure 7.



**Figure 7: FE deformation predictions compared to experimental results for aberrant case**

The true strain at the base of the specimen was correlated to the engineering strain after fitting a power law curve to the data with constants  $a = 270.4$ ,  $b = 3.861$  and  $c = 0.03373$ :

$$\varepsilon_t = a\varepsilon_{eng}^b + c \quad (8)$$

Fitting results can be seen in Figure 8, change in the shape of the curve is a result of the onset of necking – the ultimate tensile stress of the steel is exceeded and apparent softening of the material is observed at  $\sim 14\%$  engineering strain. Further to that the true strain was calculated according to the position of the material removed using Figure 9, where the values of the true strain (logarithmic strain) were obtained from the centre line of the specimen from bottom of knife edge to failure site. The corresponding radius values of the specimen were plotted alongside and thus the strain at each distance along the specimen could be calculated and verified.

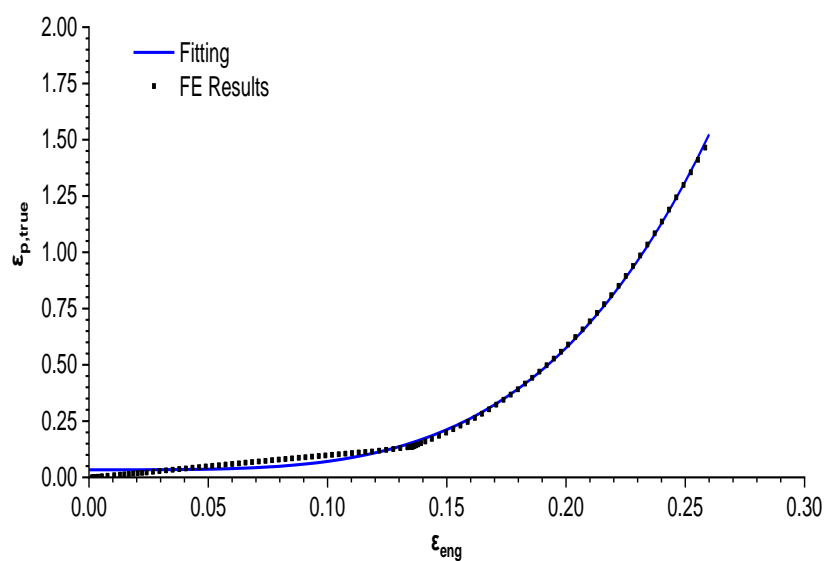


**Figure 8: Tensile test at 600°C and true vs engineering strain finite element results and power law fitting for aberrant material**

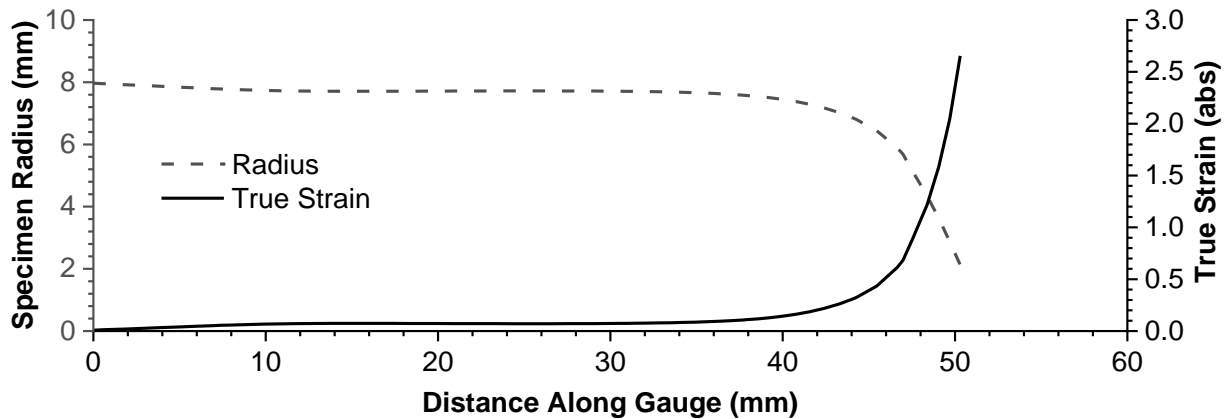


**Figure 9: Plot showing equivalent radius and logarithmic strain along centre gauge of failed specimen from FE calculations of martensitic material**

## 5. Discussion

Earlier investigation of the effect of pre-strain on subsequent creep strength in uniaxial creep specimens showed the effect to vary both with the level of pre-strain applied and with the stress in the creep test [15]. The present work has shown that the effect may also vary with the type of material tested. In the case of the normal 100% martensite material creep rate remained relatively constant with hot tensile pre-strain, whereas in the case of the aberrant 100% ferrite material creep rates decreased markedly with hot tensile pre-strain. This differing effect on creep could possibly arise because the martensitic material, which is significantly stronger than the aberrant material, has little capacity to strengthen further with additional hot tensile strain. The weaker aberrant material has a greater capacity to strengthen with additional hot tensile strain. A thorough physical understanding of the observed behaviour however requires future investigation.

Previous work has shown that at pre-straining levels >20% the Monkman-Grant correlation for the material starts to break down [6]. So even though the reduced strain rates are observed it is unclear whether the creep ductility remains the same or is reduced, as is the case for pre-straining above 20%. However, the derived  $\Phi$  parameter ( $\Phi = \dot{\epsilon}_{pmin} / \dot{\epsilon}_{omin}$ ) courtesy of Tai and Endo [19], although decreasing for the ferritic (aberrant) case, shows more complex behaviour for the martensitic case with an increasing rate for all pre-strain levels, see Figure 10 [15]. In the martensitic case the increase rate behaviour is due to the softening of the material directly after

yield, as opposed to the ferritic case where hardening is observed. The greater ductility of the ferritic material points to increased creep resistance at the strains tested.

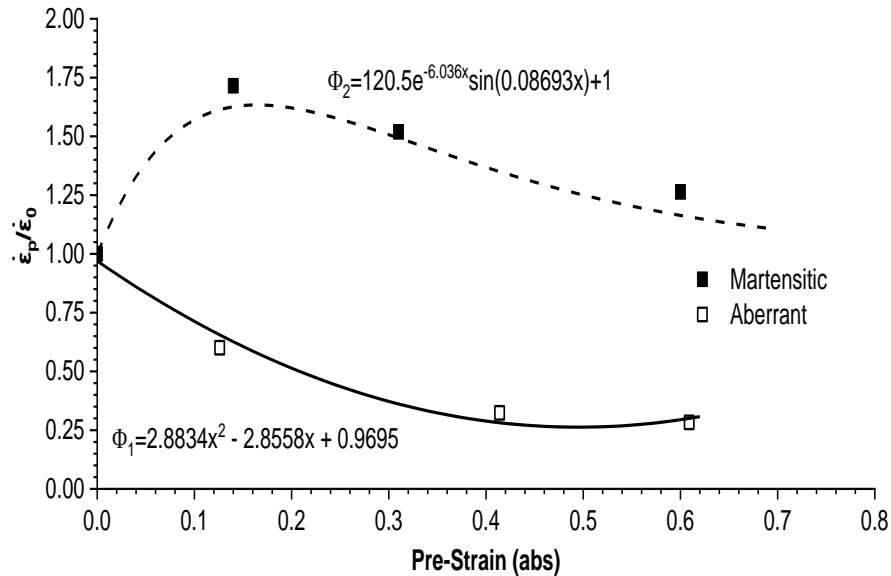


**Figure 10: Derivation of the  $\Phi$  parameter for aberrant and martensitic cases at 98MPa 600°C**

## 6. Summary and Conclusions

Impression creep testing has been carried out on small specimens removed from failed hot tensile specimens of grade 91 steel. The impression specimens have been removed at different positions along the axes of the hot tensile specimens in order to investigate the effect of hot pre-strain on creep strength. The grade 91 steel has been tested in two microstructural conditions: a normal as-manufactured condition with 100% martensite and an artificially mis heat-treated condition with 100% ferrite.

The key conclusions are:

- The two conditions show differing effects of pre-strain, with the normal condition showing little change in creep strength while the aberrant condition shows a marked increase in creep strength.
- Ferrite creep resistance increases, but at pre-strains >20% this may not translate to an increase in creep rupture strength, as evidenced in previous studies.

- Ferrite creep resistance is never greater than martensite for parameters used, Figure 6 (bottom right).

## **Acknowledgments**

This work was supported by the Engineering and Physical Sciences Research Council (EPSRC) (Grant numbers: EP/L016206/1). The funding is provided through the EPSRC Centre for Doctoral Training in Carbon Capture and Storage and Cleaner Fossil Energy ([www.ccsfe-cdt.ac.uk](http://www.ccsfe-cdt.ac.uk)). The work was also partly sponsored by the Biomass and Fossil Fuel Research Alliance (BF2RA).

C. Dyson and W. Sun would like to acknowledge the support of EPSRC, BF2RA and EPRI, and S. J. Brett would like to acknowledge the support of EPRI via Agreement 10007317.

## References

- [1] S. Chaudhuri and R. N. Ghosh, "Creep behavior of 2.25Cr1Mo steel-Effects of thermal ageing and pre-strain," *Mater. Sci. Eng. A*, vol. 510–511, no. C, pp. 136–141, 2009.
- [2] Q. Auzoux, L. Allais, C. Caës, I. Monnet, A. F. Gourgues, and A. Pineau, "Effect of pre-strain on creep of three AISI 316 austenitic stainless steels in relation to reheat cracking of weld-affected zones," *J. Nucl. Mater.*, vol. 400, no. 2, pp. 127–137, 2010.
- [3] A. Mehmanparast, C. M. Davies, D. W. Dean, and K. Nikbin, "Effects of plastic pre-straining level on the creep deformation, crack initiation and growth behaviour of 316H stainless steel," *Int. J. Press. Vessel. Pip.*, vol. 141, pp. 1–10, 2016.
- [4] A. Mehmanparast, C. M. Davies, D. W. Dean, and K. Nikbin, "Material pre-conditioning effects on the creep behaviour of 316H stainless steel," *Int. J. Press. Vessel. Pip.*, vol. 108–109, pp. 88–93, 2013.
- [5] Y. H. Zhang and D. M. Knowles, "Prestraining effect on the creep behaviour of nickel base C263 superalloy," *Mater. Sci. Technol.*, vol. 18, pp. 917–923, 2002.
- [6] D. F. Li, N. P. O'Dowd, C. M. Davies, and K. M. Nikbin, "A review of the effect of prior inelastic deformation on high temperature mechanical response of engineering alloys," *Int. J. Press. Vessel. Pip.*, vol. 87, no. 10, pp. 531–542, 2010.
- [7] H. U. Prasanna and K. R. Udupa, "Probing the deterioration of 316L stainless steel welds due to ageing and creep by indentation creep tests," *Nucl. Eng. Des.*, vol. 241, no. 12, pp. 4938–4943, 2011.
- [8] C. Dyson, W. Sun, S. J. Brett, T. H. Hyde, J. Shingledecker, and D. Purdy, "Impression Creep Testing and its Role in Component Integrity Management," in *Advances in Materials Technology for Fossil Power Plants: Proceedings of the 8th International Conference*, 2016, pp. 517–530.
- [9] W. Sun, T. H. Hyde, and S. J. Brett, "Application of Impression Creep Data in Life Assessment of Power Plant Materials at High Temperatures," *J. Mater. Des. Appl.*, vol. 222, pp. 175–182, 2008.
- [10] S. J. Brett, J. H. Rantala, and S. Holmstrom, "Practical Application of Impression Creep Data to Power Plant," in *Baltica IX: Life Management and Maintenance for Power Plants*, 2013.
- [11] T. Izaki, T. Kobayashi, J. Kusumoto, and A. Kanaya, "A creep life assessment method for boiler pipes using small punch creep test," *Int. J. Press. Vessel. Pip.*, vol. 86, no. 9, pp. 637–642, 2009.
- [12] J. R. Foulds and R. Viswanathan, "Nondisruptive material sampling and mechanical testing," *J. Nondestruct. Eval.*, vol. 15, no. 3–4, pp. 151–162, 1996.
- [13] B. Gulcimen and P. Hahner, "Determination of Creep Properties of a P91 Weldment by

- Small Punch Testing and a New Evaluation Approach," *Mater. Sci. Eng. A*, vol. 588, pp. 125–131, 2013.
- [14] CEN, "CEN-Workshop agreement 2006."
- [15] F. Cortellino, J. P. Rouse, B. Cacciapuoti, W. Sun, and T. H. Hyde, "Experimental and Numerical Analysis of Initial Plasticity in P91 Steel Small Punch Creep Samples," *Exp. Mech.*, vol. 57, no. 8, pp. 1193–1212, 2017.
- [16] F. Abe, "1 - Grade 91 heat-resistant martensitic steel ," in *Coal Power Plant Materials and Life Assessment*, A. Shibli, Ed. Woodhead Publishing, 2014, pp. 3–51.
- [17] R. K. Heywood, "Elevated Temperature Tensile Test and Microstructure/Hardness Examination of P91 Header Material - Results of Test on Material 'As Supplied from the Mill' and after 'Anomolous Heat Treatment'."
- [18] W. Sun, T. H. Hyde, and S. J. Brett, "Use of the Impression Creep Test Method for Determining Minimum Creep Strain Rate Data," in *Proceedings of the 2nd International Conference on Determination of Mechanical Properties of Materials by Small Punch and Other Miniature Testing Techniques*, 2012, pp. 297–304.
- [19] K. Tai and T. Endo, "Effect of pre-creep on the succeeding creep behavior of a 2.25Cr1Mo steel," *Scr. Metall. Mater.*, vol. 29, no. 5, pp. 643–646, 1993.